

## Crystallographic Study of a Novel Subnanomolar Inhibitor Provides Insight on the Binding Interactions of Alkenyldiarylmethanes with Human Immunodeficiency Virus-1 Reverse Transcriptase<sup>†</sup>

Matthew D. Cullen,<sup>#,‡</sup> William C. Ho,<sup>#,§</sup> Joseph D. Bauman,<sup>§</sup> Kalyan Das,<sup>§</sup> Eddy Arnold,<sup>§</sup> Tracy L. Hartman,<sup>||</sup> Karen M. Watson,<sup>||</sup> Robert W. Buckheit Jr.,<sup>||</sup> Christophe Pannecouque,<sup>⊥</sup> Erik De Clercq,<sup>⊥</sup> and Mark Cushman<sup>\*,‡</sup>

<sup>‡</sup>Department of Medicinal Chemistry and Molecular Pharmacology, School of Pharmacy and Pharmaceutical Sciences, and Purdue University Center for Cancer Research, Purdue University, West Lafayette, Indiana 47907, <sup>§</sup>Department of Chemistry and Chemical Biology, Center for Advanced Biotechnology and Medicine, Rutgers University, 679 Hoes Lane West, Piscataway, New Jersey 08854, <sup>||</sup>ImQuest Biosciences, Inc., 7340 Executive Way, Suite R, Frederick, Maryland 21704, and <sup>⊥</sup>Rega Institute for Medical Research, Katholieke Universiteit Leuven, B-3000 Leuven, Belgium. <sup>#</sup> Contributed equally to this research.

Received August 5, 2009

Two crystal structures have been solved for separate complexes of alkenyldiarylmethane (ADAM) nonnucleoside reverse transcriptase inhibitors (NNRTI) **3** and **4** with HIV-1 reverse transcriptase (RT). The structures reveal inhibitor binding is exclusively hydrophobic in nature and the shape of the inhibitor-bound NNRTI binding pocket is unique among other reported inhibitor–RT crystal structures. Primarily, ADAMs **3** and **4** protrude from a large gap in the back side of the binding pocket, placing portions of the inhibitors unusually close to the polymerase active site and allowing **3** to form a weak hydrogen bond with Lys223. The lack of additional stabilizing interactions, beyond the observed hydrophobic surface contacts, between **4** and RT is quite perplexing given the extreme potency of the compound (IC<sub>50</sub> ≤ 1 nM). ADAM **4** was designed to be hydrolytically stable in blood plasma, and an investigation of its hydrolysis in rat plasma demonstrated it has a significantly prolonged half-life in comparison to ADAM lead compounds **1** and **2**.

### Introduction

The human immunodeficiency virus (HIV), the causative agent of the acquired immune deficiency syndrome (AIDS), is a retrovirus that relies on a myriad of viral proteins to help infect CD4<sup>+</sup> cells and enable its replication. One of these proteins, reverse transcriptase (RT), facilitates viral replication by transcribing HIV's single-stranded, RNA-based genome to a double-stranded DNA equivalent that is compatible with the host cell's replication machinery. The genomic transcription abilities of RT are made possible by both the DNA polymerase and RNase H activities, which are absolutely required for the virulence and replication of HIV.<sup>1</sup> As such, RT is an attractive target for antiviral therapy, with an array of drugs currently in use for the treatment of HIV infection through inhibition of RT enzymatic function.

Structurally, RT is a heterodimeric protein composed of 66 and 51 kDa subunits (known as p66 and p51, respectively), each of which consists of connection, thumb, palm, and finger domains. The four domains of the p66 and p51 subunits are identical in amino acid sequence from their N-termini for 440 residues.<sup>2</sup> However, the heavier p66 subunit bears an additional 120 residues at its C-terminus, which form the RNase H domain. Despite their nearly identical sequences, the p66 and p51 subunits have surprisingly different ternary structures, which result in RT assuming the shape of a hand that is

capable of grasping genomic material for enzymatic processing.<sup>3</sup>

As previously mentioned, several antiretroviral drugs have been developed to inhibit RT, and they are classified by their mechanism of action.<sup>4–7</sup> The nucleoside/nucleotide reverse transcriptase inhibitors (NRTIs/NtRTIs)<sup>a</sup> halt RT's polymerase activity by acting as dNTP mimics that, when incorporated into viral DNA, terminate synthesis of the viral DNA chain.<sup>8,9</sup> The other category of HIV-1 RT inhibitors, non-nucleoside reverse transcriptase inhibitors (NNRTIs), bind to a hydrophobic, allosteric site located ~10 Å from the polymerase active site. When NNRTIs, such as nevirapine<sup>10</sup> and efavirenz,<sup>11</sup> bind to this hydrophobic site, the native arrangement of amino acid side chains is forced to change such that several of the residues point toward or intrude upon the polymerase active site.<sup>3,12</sup> In fact, crystallographic studies on various HIV-1 RT–NNRTI complexes have shown that binding of the inhibitors causes significant conformational changes within RT, primarily through the displacement of sheets β12–14 in the DNA primer grip, resulting in the enzyme binding DNA in a nonproductive manner.<sup>3,12</sup> Because of their usually tolerable toxicities, NNRTIs have enjoyed increased use in highly active antiretroviral therapy (HAART) in recent years. However, the clinical efficacy of these inhibitors has been attenuated by the emergence of drug-resistant HIV-1 strains that bear mutant forms of RT.<sup>6,13</sup>

<sup>†</sup>PDB code for **3** with HIV-1 RT, 3IS9; PDB code for **4** with HIV-1 RT, 3IRX.

\*To whom correspondence should be addressed. E-mail: cushman@pharmacy.purdue.edu. Phone: 765-494-1465. Fax: 765-494-6790.

<sup>a</sup>Abbreviations: ADAM, alkenyldiarylmethane; HAART, highly active antiretroviral therapy; NNRTI, nonnucleoside reverse transcriptase inhibitor; NRTI, nucleoside reverse transcriptase inhibitor; NtRTI, nucleotide reverse transcriptase inhibitor; TI, therapeutic index.

**Table 1.** Antiviral Activity and Hydrolysis Half-Lives of ADAMs 1–4

compd	IC <sub>50</sub> (μM) <sup>a</sup>	EC <sub>50</sub> (μM) <sup>b</sup>			CC <sub>50</sub> (μM) <sup>c</sup>		half-life <i>t</i> <sub>1/2</sub> ± SD (min) <sup>d</sup>
		HIV-1 <sub>RF</sub>	HIV-1 <sub>IIB</sub>	HIV-2 <sub>ROD</sub>	CEM-SS	MT-4	
<b>1</b> <sup>g</sup>	0.30	0.1	0.3	NA <sup>e</sup>	13	91	6.2 ± 0.4
<b>2</b> <sup>h</sup>	0.02	0.03	0.09	NA <sup>e</sup>	5.1	17	1.3 ± 0.09
<b>3</b> <sup>i</sup>	0.38	0.7	0.8	NA <sup>e</sup>	17	> 100	12.4 ± 0.7 <sup>f</sup>
<b>4</b>	< 0.001	0.07	0.18	NA <sup>e</sup>	3.0	3.9	238 ± 8.5

<sup>a</sup> Inhibitory activity versus HIV-1 RT with poly(rC)·oligo(dG) as the template/primer. <sup>b</sup> EC<sub>50</sub> is the 50% inhibitory concentration for inhibition of the cytopathic effect of HIV-1<sub>RF</sub> in CEM-SS cells, HIV-1<sub>IIB</sub> in MT-4 cells, or HIV-2<sub>ROD</sub> in MT-4 cells. <sup>c</sup> CC<sub>50</sub> is the cytotoxic concentration required to induce cell death for 50% of the mock-infected CEM-SS or MT-4 cells. <sup>d</sup> Metabolic half-life of the compound when it was incubated with rat plasma; determined from a minimum of two replicates. <sup>e</sup> Not active. <sup>f</sup> Previously reported in ref 18. <sup>g</sup> Reference 17. <sup>h</sup> Reference 19. <sup>i</sup> Reference 18.

There is great need for the development of NNRTIs that are efficacious against both wild-type and drug-resistant forms of HIV-1 RT.

For several years, our group has been developing a series of alkenyldiarylmethane-based NNRTIs that exhibit antiviral activity against a number of the common drug-resistant strains of HIV-1 that bear RT mutations.<sup>14–20</sup> Previous hypothetical binding models developed for potent inhibitors **1** and **2** showed the alkenyldiarylmethanes (ADAMs) oriented in accordance with the “butterfly” model, as described by Schäfer, which reflects the binding orientation of NNRTIs like nevirapine, TIBO, and α-APA.<sup>16,19,21</sup> However, these models are not sufficiently general for the ADAM class of inhibitors, nor do they correlate with the RT SAR. It is well-known that the NNRTI binding pocket is plastic in nature and will conform to the structure of the specific inhibitor that is bound, thus making molecular modeling studies problematic. Recent crystallographic studies involving new structural classes of NNRTIs have revealed compounds that are highly flexible (large number of rotatable bonds) and similar in structure and can each bind to RT in different orientations.<sup>22,23</sup> Furthermore, potent inhibitors can even have more than one binding orientation if the structure is flexible enough to allow for “wiggling” and “jiggling” inside the binding pocket.<sup>22,23</sup> Yet, the malleable nature of the NNRTI binding pocket obviates attempts to generate an accurate binding model via de novo methods.

Given that current ADAM–RT interaction models lack correlation with SAR data, our desire to identify key protein–ligand interactions for this class of NNRTIs necessitated the acquisition of ADAM–RT crystal structures. Herein we reveal the first X-ray crystal structures of HIV-1 RT in complex with an ADAM (compounds **3** and **4**). The present report also discloses the synthesis and antiviral evaluation of the incredibly potent NNRTI **4** (IC<sub>50</sub> ≤ 1 nM). ADAM **4** was designed as part of an investigative effort to replace the enzymatically labile methyl esters in lead compound **1** with bioisosteres that would confer hydrolytic stability in blood plasma while maintaining the desired pharmacological activity.

## Results and Discussion

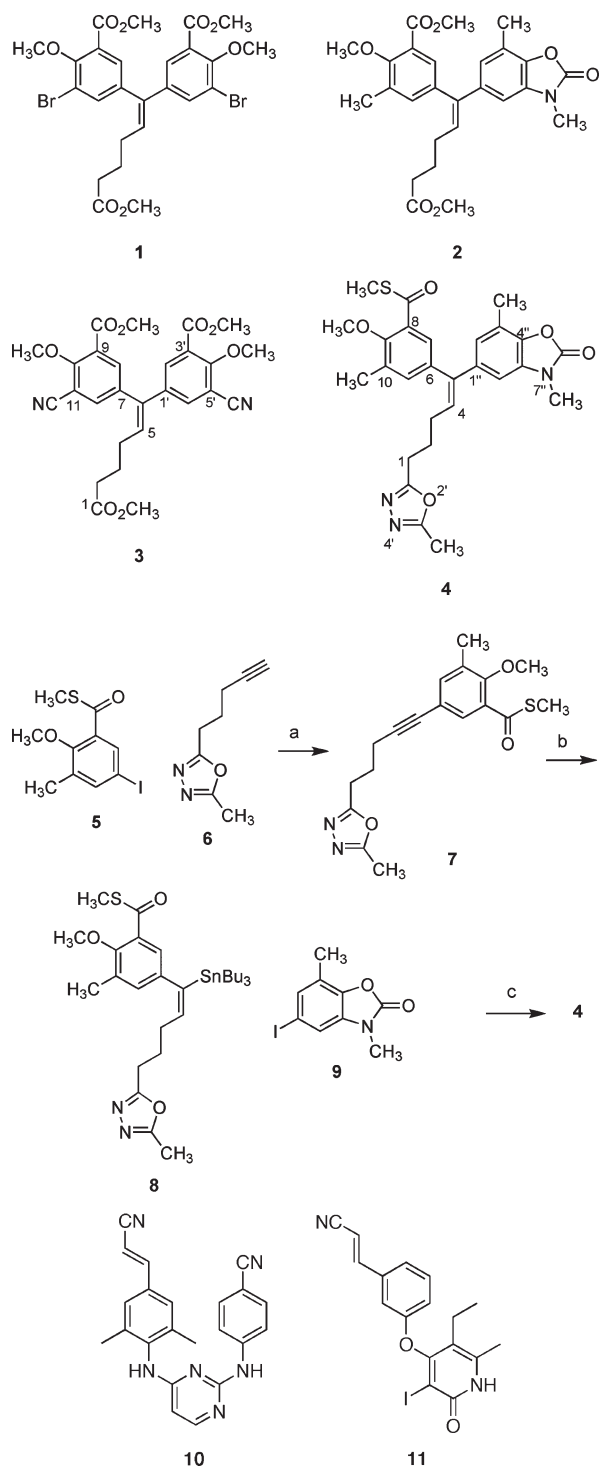
**Chemistry.** Several routes for the synthesis of ADAM analogues have been reported.<sup>17,24,25</sup> The synthesis of ADAM **3** has been previously described.<sup>26</sup> The synthesis of compound **4** centers on a series of palladium-catalyzed cross-coupling reactions recently utilized to prepare a set of hydrolytically stable ADAM analogues.<sup>20</sup> Briefly, the synthesis of ADAM **4** began with the coupling of known compounds **5** and **6** under standard Sonogashira conditions (Scheme 1). Cross-coupling product **7** was treated with tributyltin hydride and Pd(PPh<sub>3</sub>)<sub>4</sub> to obtain stannane **8**,<sup>20</sup>

which was elaborated with iodide **9**<sup>20</sup> through the Stille reaction to afford ADAM **4**.

**Evaluation of RT Inhibition, Antiviral Activity, and Hydrolytic Stability.** As is standard in our investigations, ADAM **4** was evaluated in a functional enzyme assay for inhibition of HIV-1 RT. Additionally, the cytotoxicity and ability of ADAM **4** to protect cells from the cytopathic effects of HIV-1<sub>RF</sub>, HIV-1<sub>IIB</sub>, or HIV-2<sub>ROD</sub> were evaluated. The metabolic half-life of **4** in rat plasma was also determined in a metabolic stability assay. The results of the RT inhibitory, antiviral, metabolic, and cytotoxicity analyses for ADAM **4** are presented in Table 1. Associated data for compounds **1**–**3** are included in Table 1 for comparison.<sup>17–19</sup>

Concerning inhibition of RT enzymatic activity, ADAM **4** is the most potent analogue among the four compounds under discussion, exhibiting an impressive IC<sub>50</sub> of less than or equal to 1 nM. The detection limits of our functional enzyme assay precluded a more exact IC<sub>50</sub> determination for **4**. Despite ADAM **4**'s remarkable potency in the in vitro assay, the manifestation of this analogue's cytoprotective efficacy in whole cells is surprisingly lower than expected and comparable to that of ADAM **1** (IC<sub>50</sub> = 0.3 μM). The discrepancy between ADAM **4**'s enzyme inhibitory potency and its cytoprotective activity could be the result of many factors, including the fact that the enzymatic assay, in contrast to the cellular system, uses the synthetic template/primer poly(rC)·oligo(dG). Significant cytotoxicity is observed for each of the analogues with ADAM **4** unfortunately presenting the narrowest therapeutic index (TI ≈ 32). Because the current goal of our research is to improve on the metabolic stability of the ADAMs through isosteric replacement of enzymatically labile methyl esters, ADAM **4** was evaluated in our rat blood plasma stability assay, and the results were compared to previous leads (ADAM **1**). ADAM **4** was found to be at least 40-fold more stable (*t*<sub>1/2</sub> = 238 min) than **1**, indicating the fused oxazolidinone and oxadiazole isosteres rendered **4** less prone to enzymatic degradation.

As our initial interest in studying the ADAM scaffold was spurred by the ability of initial leads to retain antiviral activity against several common NNRTI-resistant HIV-1 strains, the antiviral activity of **4** was evaluated against NNRTI-resistant HIV strains. Specifically, CEM-SS cells infected with HIV-1 strain NL4-3 which bore either the K103N or Y181C RT mutant were treated with ADAM **4** to determine the residual cytoprotective activity of the inhibitor. The results of the experiment are presented in Table 2, with data for ADAM **1** and nevirapine included for comparison. Unlike that of ADAM **1**, the cytoprotective activity of **4** was completely abolished (EC<sub>50</sub> > 100 μM) by two of the most common NNRTI resistance mutations, K103N and Y181C. A priori one would have expected ADAM **4** to exhibit moderate antiviral activity,

Scheme 1<sup>a</sup>

<sup>a</sup> Reagents and conditions: (a) cat. PdCl<sub>2</sub>(PPh<sub>3</sub>)<sub>2</sub>, cat. CuI, Et<sub>3</sub>N, THF; (b) cat. Pd(PPh<sub>3</sub>)<sub>4</sub>, Bu<sub>3</sub>SnH, THF, 0 °C; (c) cat. Pd(PPh<sub>3</sub>)<sub>4</sub>, cat. CuI, CsF, DMF, 60 °C.

even in the presence of the two mutations, on the basis of the point mutation data for ADAM **1**. Such a drastic change in activity suggests that ADAM **4** is incapable of adapting conformationally to the structural changes induced in the NNRTI binding pocket by the K103N and Y181C mutations, whereas the slightly more flexible ADAM **1** can adopt an alternative binding conformation or orientation.

**Table 2.** Antiviral Activity of ADAMs **1** and **4** against NNRTI-Resistant HIV-1 Strains

compd	EC <sub>50</sub> (μM) <sup>a</sup>		
	WT <sup>b</sup>	K103N <sup>c</sup>	Y181C <sup>d</sup>
<b>1</b> <sup>f</sup>	0.1	0.42	6.1
<b>4</b>	0.7	> 100	> 100
nevirapine	NT <sup>e</sup>	0.6	0.8

<sup>a</sup> EC<sub>50</sub> is the 50% inhibitory concentration for inhibition of the cytopathic effect of HIV-1<sub>RF</sub> in CEM-SS cells. <sup>b</sup> Cytoprotective activity against HIV-1<sub>RF</sub> bearing wild-type reverse transcriptase. <sup>c</sup> Cytoprotective activity against HIV-1 bearing reverse transcriptase containing the K103N mutation. <sup>d</sup> Cytoprotective activity against HIV-1 bearing reverse transcriptase containing the Y181C mutation. <sup>e</sup> Not tested. <sup>f</sup> Data were taken from ref 16.

**ADAM-RT Complex Structure and Analysis.** The ADAM-RT structures were determined at final resolutions of 2.6 and 2.8 Å for compounds **3** and **4**, respectively, with associated diffraction and refinement data presented in Table 3. The overall conformation of RT in the crystal structures is typical of most NNRTI-RT complexes (Figure 1) in which the p66 thumb region is hyperextended. The side chains of Tyr181, Tyr188, and Trp229 are rotated or shifted toward the polymerase active site, and the β12–14 sheet is displaced by approximately 2 Å relative to the structure of apo-RT.

In general, both **3** and **4** occupy nearly the entire volume of the NNRTI-binding pocket, making very few, if any, polar contacts with the protein (Figure 2). The latter observation is surprising but not unprecedented given the recent crystal structure of the highly potent NNRTI, TMC278 (**10**), which showed that drastic improvements in potency were achieved by the addition of an increased number of hydrophobic interactions.<sup>27</sup> Although the NNRTI-binding pocket is known to be predominantly hydrophobic in nature and known nonnucleoside inhibitors have significant hydrophobic character, most NNRTI-RT complexes, including **10**, exhibit one or more hydrogen bonds between the inhibitor and protein. Our past SAR studies indicated the ester functionalities are a crucial component of the ADAM pharmacophore and were suspected of participating in one or more hydrogen bonds with RT.

In comparing the NNRTI-binding pockets containing **3** and **4** to those of other published NNRTI-RT crystal structures, it was observed that the shape of the ADAM-binding pocket resembles that of the bis(heteroaryl)-piperazine (BHAP) series, to which delavirdine belongs. For NNRTI binding, it is commonly accepted that inhibitors bind to one of two NNRTI-binding pocket “shapes”, one of which is represented by nevirapine (PDB code 1VRT) and the other, delavirdine (PDB code 1KLM). The nevirapine-binding pocket is characterized as small and encapsulating, where no surface gaps are observed in the pocket. In the case of delavirdine, the inhibitor is quite large and the NNRTI-binding pocket expands to accommodate its volume. The binding pocket acquires additional space by breaking the hydrogen bond between the carbonyl of Pro236 and main chain amide of Lys101, which creates a large gap in the pocket near the surface of the protein. Additionally, the β12–14 sheets are displaced further than in the nevirapine pocket, which provides supplementary volume and results in the opening of another gap toward the back of the pocket. The aforementioned hole in the back of the binding pocket is significantly larger in the two ADAM structures, relative to

**Table 3.** Crystallographic Data Collection and Structural Refinement Statistics

	RT/ADAM 3	RT/ADAM 4
Crystallographic Data		
space group	C2	C2
<i>a</i> , <i>b</i> , <i>c</i> (Å)	162.82, 73.73, 108.69	164.64, 75.39, 110.66
$\beta$ (deg)	99.55	100.08
resolution range (Å)	50–2.55	50–2.8
total no. of reflections	486 221	362 418
no. of unique reflections	41 074	28 872
$R_{\text{merge}}^{a,b}$	0.086 (0.512)	0.091 (0.368)
$I/\sigma^d$	18.3 (3.0)	10.1 (1.8)
completeness (%) <sup>a</sup>	98.7 (100.0)	87.2 (92.6)
Refinement		
no. of reflections in $R_{\text{free}}$ set	1 677	1 414
$R_{\text{work}}^c$	25.34	23.62
$R_{\text{free}}^c$	28.27	28.86
rmsd bond lengths (Å)	0.008	0.010
rmsd angles (deg)	1.281	1.325
av <i>B</i> factor of protein atoms (Å <sup>2</sup> )	82	91
av <i>B</i> factor of inhibitor atoms (Å <sup>2</sup> )	84	74
no. of protein atoms	7933	7941
no. of inhibitor atoms	37	36
no. of water atoms	126	0

<sup>a</sup>Numbers in parentheses denote statistics for last resolution shell.

<sup>b</sup> $R_{\text{merge}} = \sum_h \sum_i |I_{h,j} - I_h| / \sum_h \sum_i I_{h,i}$ , where  $I_h$  is the mean intensity of symmetry-related reflections. <sup>c</sup> $R_{\text{work}} = \sum ||F_o| - |F_c|| / \sum |F_o|$ , where  $F_o$  and  $F_c$  are the observed and calculated structure factor amplitudes, respectively. <sup>d</sup> $R_{\text{free}} = \sum ||F_o| - |F_c|| / \sum |F_o|$  for reflections in the test set.

the delavirdine structure, and allows both inhibitors to protrude from the pocket, placing them unusually close to the RT polymerase site (Figure 3). In fact, the 5' nitrile functionality on ADAM 3 is held only 6 Å, with an unobstructed "line-of-site", from the catalytically active residue Asp186 in the polymerase active site! The previous observation can only be made for the crystal structure of aryloxy pyridinone R165481 (**11**) (PDB code 2B5J), which shows the nitrile of the ligand lays only 4.9 Å from aspartate 186.<sup>28</sup> In comparison to the nevirapine and delavirdine structures, the shortest paths from each inhibitor to Asp186 are 8.6 and 8.9 Å in length, respectively, where the paths are obstructed by Y181 and Y188.

A more detailed analysis of the structures revealed that ADAM 4 creates a smaller pocket and binds slightly deeper relative to 3. Yet in both crystals the alkenyl side chains of the ADAMs display significant edge-to-face interactions with the aromatic rings of Tyr181, Tyr188, and Trp229, in addition to general hydrophobic interactions with the side chains of Leu100 and Leu234. Most notably, the vinyl hydrogen on each ligand is nearly buried in the  $\pi$  cloud of Trp229's indole ring. The Trp229 residue is highly conserved among HIV strains and is part of the DNA/RNA primer grip, thus disrupting the alignment of this residue that can significantly impair RT polymerase activity.<sup>29–31</sup> The aryl rings situated trans to the side chain in both ligands are buried deep in the pocket and occupy a region normally blocked by residues Phe227, Trp229, and Tyr188. With 3 and 4 bound so deeply in the pocket, the side chain of Phe227 becomes pinned against the peptide backbone, forcing a chain rotation of the local residues (219–228). This chain displacement opens a large hole at the back of the binding pocket and, in the case

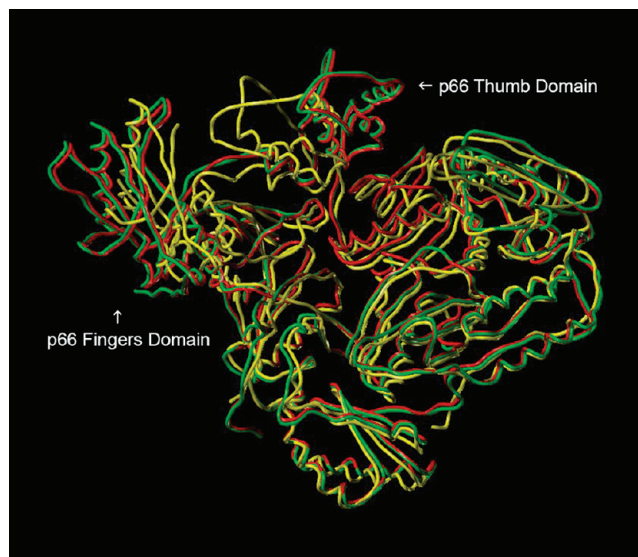


**Figure 1.** An overlay of the backbone tube structures of unliganded apo-RT (1HMY, yellow), the RT/3 complex (red), and the RT/4 complex (green). The crystal structures obtained for the RT/3 and RT/4 complexes show hyperextension of the thumb region and displacement of the fingers, relative to the structure of unliganded apo-RT. In areas of very close overlap, the red and green tubes appear as either red or green.

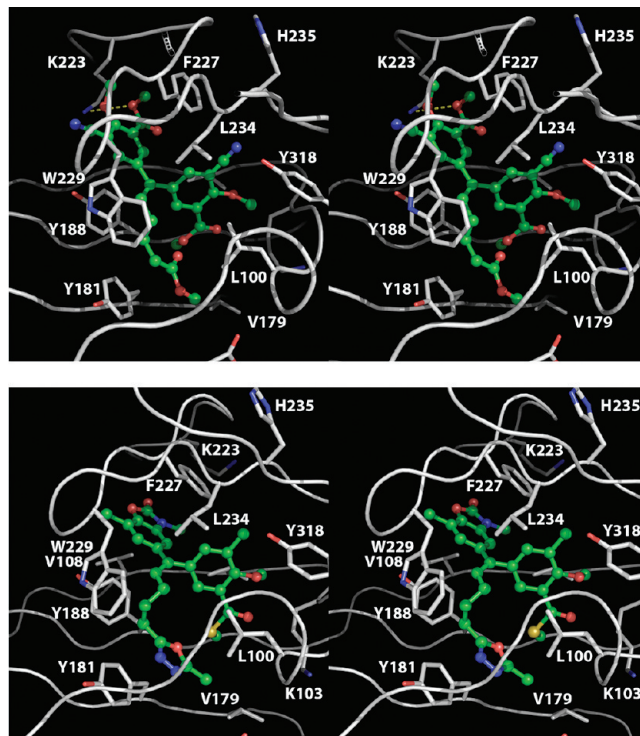


**Figure 2.** (Top) Depiction of the NNRTI-binding pocket obtained from the RT/ADAM 3 crystal structure. (Bottom) Depiction of the NNRTI-binding pocket obtained from the RT/ADAM 4 crystal structure. The view for each panel is from the "front side" of the binding pocket, from the point of view of the putative solvent channel through which NNRTIs are believed to enter. The stereo-view is programmed for wall-eyed viewing.

of ADAM 3, brings the side chain of Lys223 in close proximity to the "trans" aryl ring's ester. The proximity of Lys223 hints at a potential hydrogen bond, but the interatomic distance of 3.6 Å from the side chain amine to the

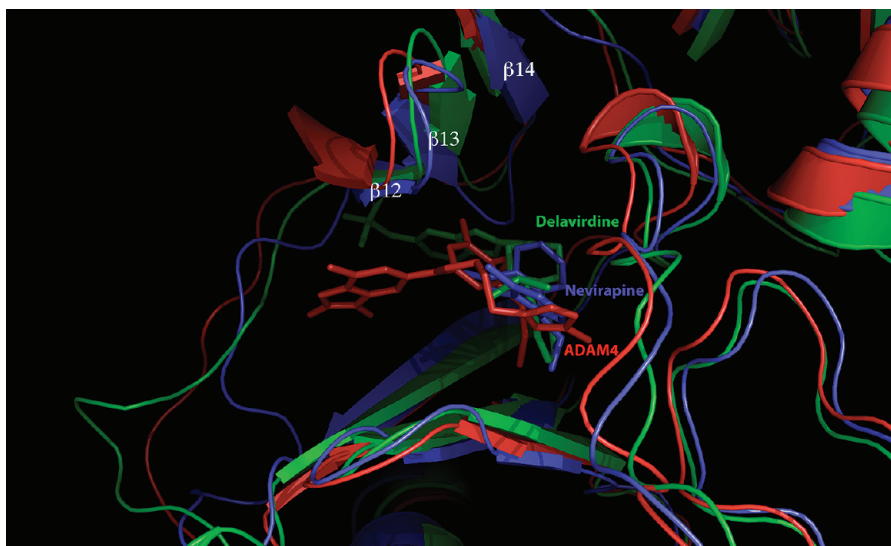


**Figure 3.** Overlay of the crystal structures of RT bound to ADAM 4 (red), nevirapine (blue), and delavirdine (green). The NNRTI binding pocket is more compact when nevirapine is bound in contrast to a more open pocket when delavirdine or ADAM 4 are present;  $\beta$ 12,  $\beta$ 13, and  $\beta$ 14 are rearranged to make room for the larger inhibitors.

nearest ether-type oxygen of **3** is at the outer limits of hydrogen-bonding distance. In comparison, electron density for residues 218–223 in the RT/ADAM 4 crystal structure is completely absent, suggesting a large degree of disorder in this region of the protein. Such an observation precludes the assignment of a hydrogen bond between **4** and Lys223 in the crystal structure; however, such an association may theoretically arise under physiological conditions.

Further analysis of the crystal structures shows stacking between the aromatic ring of Tyr181 and the terminal side chain functionalities of the ligands in both structures. Additionally, the methyl ester (ADAM 3) and oxazolone (ADAM 4) moieties on the ADAM rings oriented trans to the side chains show similar stacking interactions with the aromatic side chain of Phe227. Given the observed stacking interactions between the methyl ester of **3** and Phe227, replacement of this functional group by the cyclic oxazolone in **4** may have the benefit of rigidifying the atoms in the proper planar orientation for  $\pi$ -stacking with Phe227. This may be one reason for the increased potency of **4**. It is interesting to note that the  $IC_{50}$ 's of ADAMs **2** and **4** differ by over an order of magnitude with **4** being the more potent of the two. The major difference between **2** and **4** is that **2** retains the methyl ester on the end of its alkenyl arm, while **4** has an oxadiazole in this place. If **2** and **4** bind to RT in a similar fashion, the  $\pi$ -stacking with Tyr181 (which is also observed in the cocrystal structure of **3**) should be retained. However, **4** has the benefit of a rigidified, planar heterocycle for this stacking interaction while **2** retains the methyl ester.

The aromatic rings of **3** and **4** that are oriented cis to the side chains are cradled by the hydrophobic residues Leu100, Val106, Val179, and Leu234. The protein–ligand interactions described for both structures are primarily hydrophobic in nature and help in explaining why the carboxylate analogues, derived from hydrolysis of the ADAM esters, are biologically inactive.

With regard to the point mutation data for ADAMs **1** and **4**, the application of information gleaned from the two ADAM–RT crystal structures leads to several interesting observations and conclusions on the data. In the case of ADAM 4, given the significant edge-to-face and van der

Waals contacts between the inhibitor and Tyr181 residue, it is unsurprising that mutation of this residue significantly impacts the antiviral activity of **4**. However, the crystal structure shows no specific interactions between **4** and Lys103, suggesting conformational changes in the binding pocket residues lead to attenuation of **4**'s antiviral activity. If one were to assume ADAM 1 binds to RT in a manner similar to **3**, then ADAM 1 would exhibit many of the same binding interactions with RT as are observed for ADAM 4. Yet, the point mutation data indicate that modulating the shape of the NNRTI binding pocket via replacement of the Tyr181 and Lys103 residues results in small to moderate changes in the affinity of **1** for HIV-1 RT. This observation can be rationalized in two ways: (1) ADAM 1 binds to RT in an orientation vastly different from **3** and **4**, making analyses based on the two ADAM–RT crystal structures impossible; (2) because **1** possesses more conformational flexibility relative to **4**, the former analogue is capable of adopting a favorable, alternative binding conformation. In the absence of additional crystallographic or accurate modeling data for ADAM 1, validation of either scenario is problematic.

**Conclusion.** Described herein are the first crystal structures of HIV-1 RT in complex with two ADAM NNRTIs. Of the two inhibitors discussed, ADAM 4 has been identified as a subnanomolar inhibitor of HIV-1 RT enzymatic activity in vitro, and the synthesis of this compound has been outlined. Interestingly, the crystal structures for the ADAM complexes reveal that inhibitors **3** and **4**, which differ in enzymatic inhibitory activity by at least 2 orders of magnitude, exhibit nearly identical binding orientations and interactions with the NNRTI-binding pocket. Moreover, the binding interactions observed in the protein–inhibitor complexes are exclusively hydrophobic in nature with additional  $\pi$ -stacking attractions. The deep binding exhibited by **3** and **4** allows the inhibitors to protrude through the back of the NNRTI binding pocket and into the polymerase active site, making the ADAMs unique among other published NNRTI–RT complexes. The former observation has led to the hypothesis that it may be possible to tether an ADAM to a traditional nucleoside/nucleotide inhibitor (e.g., AZT, tenofovir), generating a dual inhibitor that may simultaneously

bind to the NNRTI and NtRTI and polymerase binding sites. Such a compound would undoubtedly be an extremely potent RT inhibitor and potential antiviral agent.

### Experimental Section

All  $^1\text{H}$  NMR spectra were obtained at 300 MHz in  $\text{CDCl}_3$ , using the residual  $\text{CHCl}_3$  resonance as the internal standard for chemical shifts. A Perkin-Elmer 1600 series FT-IR spectrometer was used to record infrared spectra of all compounds. Preparative TLC separations utilized Analtech Uniplates with glass-supported silica ( $20 \times 20$  cm, 2000  $\mu\text{m}$  thickness) and UV indicator (254 nm). The progress of reactions was monitored with Bakerflex silica gel IB2-F plates (0.25 mm thickness). Unless specifically mentioned, chemicals and solvents were of minimum reagent grade and used as obtained from commercial sources without further purification. Anhydrous tetrahydrofuran was prepared by distillation from sodium-benzophenone ketal radical. The hydrolytic stability assay utilized lyophilized rat plasma (lot no. 065K7555) from Sigma Chemical Co., St. Louis, MO. Elemental analyses were performed at the Purdue University Microanalysis Laboratory. All yields reported refer to isolated yields. Elemental analysis established >95% purity of ADAM 4.

(*E*)-*S*-Methyl 5-(1-(3,7-Dimethyl-2-oxo-2,3-dihydrobenz[*d*]oxazol-5-yl)-5-(5-methyl-1,3,4-oxadiazol-2-yl)pent-1-enyl)-2-methoxy-3-methylbenzothioate (4). An oven-dried flask was charged with stannane **8**<sup>20</sup> (202 mg, 0.319 mmol) and iodide **9**<sup>19</sup> (140 mg, 0.533 mmol). Anhydrous DMF (3 mL) was added via a syringe, and the resulting mixture was sparged with argon for 10 min. Cesium fluoride (195 mg, 1.28 mmol), Pd(PPh<sub>3</sub>)<sub>4</sub> (38 mg, 0.033 mmol), and copper(I) iodide (16 mg, 0.084 mmol) were quickly weighed and added to the flask in the order listed. The reaction mixture was allowed to stir at 60 °C, under an argon atmosphere, for 14 h. The system was allowed to cool to room temperature, and the reaction mixture was diluted with ethyl acetate (5 mL), water (1 mL), and methanol (1 mL). The mixture was sonicated at room temperature (30 s) and filtered through a pad of silica (10 mL). The filter pad was washed with ethyl acetate (50 mL), and the filtrate was washed with 1.0 M ethylenediaminetetraacetic acid solution (pH = 10, 2 × 20 mL) and saturated ammonium chloride solution (2 × 20 mL). The phases were separated, and the organic phase was dried over magnesium sulfate, filtered, and condensed in vacuo. The crude products were purified by preparative thin-layer chromatography using ethyl acetate as the eluant. The desired product was further purified, two more times, by preparative thin-layer chromatography for which 66% ethyl acetate–hexanes was used as the developing solution for the first plate and 80% ethyl acetate–toluene was used for the second. The desired product was isolated as an opaque oil (6 mg, 4%). IR (neat) 2929, 2862, 1777, 1675, 1641, 1595, 1570, 1472, 1367, 1333, 1303, 1245, 1227, 1149, 1123, 1044, 1002  $\text{cm}^{-1}$ ;  $^1\text{H}$  NMR (300 MHz,  $\text{CDCl}_3$ )  $\delta$  7.37 (d,  $J = 2.1$  Hz, 1 H), 7.08 (d,  $J = 2.1$  Hz, 1 H), 6.74 (s, 1 H), 6.57 (s, 1 H), 5.97 (t,  $J = 7.5$  Hz, 1 H), 3.88 (s, 3 H), 3.35 (s, 3 H), 2.82 (t,  $J = 7.5$  Hz, 2 H), 2.47 (s, 3 H), 2.45 (s, 3 H), 2.33 (s, 6 H), 2.25 (q,  $J = 7.5$  Hz, 2 H), 1.95 (p,  $J = 7.5$  Hz, 2 H); ESIMS  $m/z$  (relative intensity) 530 ( $\text{MNa}^+$ , 24), 508 ( $\text{MH}^+$ , 3), 478 ( $\text{MH}^+ - \text{SCH}_3 + \text{H}_2\text{O}$ , 100). Anal. Calcd for  $\text{C}_{27}\text{H}_{29}\text{N}_3\text{O}_5\text{S}$ : C, 63.89; H, 5.76; N, 8.28. Found: C, 63.60; H, 5.96; N, 7.91.

**Crystallography.** All crystallography experiments utilized an RT construct (RT52A) specifically optimized to cocrystallize with NNRTIs.<sup>32</sup> RT was purified as described previously, concentrated to 40 mg/mL, then flash frozen, and stored at  $-80$  °C. Prior to use, RT was allowed to thaw on ice and then diluted to a final concentration of 20 mg/mL in 10 mM Tris, pH 8.0, and 75 mM NaCl. ADAM inhibitors were added to RT at a stoichiometry of 1:1.5 protein:inhibitor from stock solutions previously dissolved in DMSO. Inhibitor and protein were allowed to incubate at room temperature for 10 min and then returned on ice. Crystals were grown using the vapor diffusion

method by mixing 1  $\mu\text{L}$  of protein–inhibitor complex and 1  $\mu\text{L}$  of mother liquor sealed over a 500  $\mu\text{L}$  reservoir solution. The best crystals appeared at 4 °C using a mother liquor consisting of 50 mM imidazole, pH 6.4, 10% PEG 8000, 100 mM ammonium sulfate, 10 mM spermine, and 30 mM magnesium sulfate. Crystals were harvested and flash cooled in liquid nitrogen after transferring to mother liquor supplemented with 25% ethylene glycol. Data were collected at the Cornell High Energy Synchrotron Source (CHESS) F1 beamline. The program HKL2000<sup>33</sup> was used to index, scale, and merge reflection data. The phase problem was solved by molecular replacement using the program Molrep and the protein coordinates of the RT52A/10 complex (PDB code 2ZD1) as the starting model.<sup>34</sup> Upon initial examination of the difference Fourier density, the presence of each respective inhibitor was clear. Refinement of protein coordinates proceeded by iterative rounds of manual fitting of electron density using the program COOT<sup>35</sup> followed by reciprocal space refinement using CNS.<sup>36</sup> In the final stages of model refinement, as the  $R_{\text{work}}$  and  $R_{\text{free}}$  converged, the respective inhibitors were built into the electron density and subjected to coordinate and  $B$ -factor minimization.

**RT Inhibition Assay.** The ability of ADAM 4 to inhibit the enzymatic activity of recombinant HIV-1 RT (p66/51 dimer) was evaluated as previously described.<sup>24,37</sup> Briefly, inhibition of purified HIV-1 reverse transcriptase was determined by the amount of  $^{32}\text{P}$ -labeled GTP incorporated into a nascent DNA strand, with a poly(rC)·oligo(dG) homopolymer primer, in the presence of increasing concentrations of the target compounds.

**In Vitro Antiviral Assays.** The antiviral activity of ADAM 4 was determined for the HIV strains HIV-1<sub>RF</sub>, HIV-1<sub>IIB</sub>, and HIV-2<sub>ROD</sub>. The antiviral activity against HIV-1<sub>RF</sub> and NNRTI-resistant strains (Y181C/K103N) was determined in infected CEM-SS cells using the XTT cytoprotection assay, as previously described.<sup>37</sup> Evaluation of antiviral activity against the HIV-1<sub>IIB</sub> and HIV-2<sub>ROD</sub> strains was performed in infected MT-4 cells using the previously described MTT assay.<sup>18,38</sup>

**In Vitro Hydrolytic Stability Assay Utilizing Rat Plasma.** ADAM 4 was tested for its hydrolytic stability in solutions of reconstituted rat plasma using methods that have been previously reported.<sup>18</sup> The internal standard used was 1,1-diphenylethylene, and rat plasma from Sigma was utilized for the experiments (lot no. 065K7555). The aliquot supernatants were analyzed using a Waters binary HPLC system (Model 1525, 20  $\mu\text{L}$  injection loop) and a Waters dual wavelength absorbance UV detector (Model 2487) set for 254 nm. Data were collected and processed using the Waters Breeze software (version 3.3) on a Dell Optiplex GX280 personal computer. The mobile phase consisted of 8:2 (v/v) acetonitrile–water, and the Symmetry HPLC column (4.6 mm × 150 mm) was packed with C<sub>18</sub> silica from Waters. The column was maintained at room temperature during the analyses. The reported half-life is an average calculated from two replicates. Half-lives for the individual replicates were calculated from regression curves fitted to plots of the compound concentration versus time.

**Acknowledgment.** This investigation was made possible by funding from the National Institutes of Health, DHHS, through Grant RO1-AI-43637, and research was conducted in a facility constructed with the financial support of a Research Facilities Improvement Program Grant, No. C06-14499, also from the National Institutes of Health. E.A.'s laboratory is supported by NIH Grant AI 27690 MERIT Award and F32GM084726 (W.C.H.).

### References

- Cheng, Y. C.; Gao, W. Y.; Chen, C. H.; Vazquez-Padua, M.; Starnes, M. C. DNA Polymerases Versus HIV Reverse Transcriptase in AIDS Therapy. *Ann. N.Y. Acad. Sci.* **1990**, *616*, 217–223.
- Jacobo-Molina, A.; Ding, J.; Nanni, R. G.; Clark, A. D., Jr.; Lu, X.; Tantillo, C.; Williams, R. L.; Kamer, G.; Ferris, A. L.; Clark, P.

- Hizi, A.; Hughes, S. H.; Arnold, E. Crystal Structure of Human Immunodeficiency Virus Type I Reverse Transcriptase Complexed with Double-Stranded DNA at 3.0 Å Resolution Shows Bent DNA. *Proc. Natl. Acad. Sci. U.S.A.* **1993**, *90*, 6320–6324.
- (3) Rodgers, D. W.; Gamblin, S. J.; Harris, B. A.; Ray, S.; Culp, J. S.; Hellmig, B.; Woolf, D. J.; Debouck, C.; Harrison, S. C. The Structure of Unliganded Reverse Transcriptase from the Human Immunodeficiency Virus Type 1. *Proc. Natl. Acad. Sci. U.S.A.* **1995**, *92*, 1222–1226.
- (4) Gulick, R. M.; Staszewski, S. New Drugs for HIV Therapy. *AIDS* **2002**, *16*, S135–S144.
- (5) De Clercq, E. New anti-HIV Agents and Targets. *Med. Res. Rev.* **2002**, *22*, 531–565.
- (6) De Clercq, E. Non-Nucleoside Reverse Transcriptase Inhibitors (NNRTIs): Past, Present, and Future. *Chem. Biodiversity* **2004**, *1*, 44–64.
- (7) De Clercq, E. New Approaches toward Anti-HIV Chemotherapy. *J. Med. Chem.* **2005**, *48*, 1297–1313.
- (8) Vivet-Boudou, V.; Didierjean, J.; Isel, C.; Marquet, R. Nucleoside and Nucleotide Inhibitors of HIV-1 Replication. *Cell. Mol. Life Sci.* **2006**, *63*, 163–186.
- (9) De Clercq, E. Nucleoside/Nucleotide Inhibitors of HIV Reverse Transcriptase. *Infect. Dis. Ther.* **2003**, *30*, 485–504.
- (10) Tappa, H. D.; Chang, R. S.; Smith, K. M. Isolation, Purification, and Partial Characterization of Prunellin, an Anti-HIV Component from Aqueous Extracts of *Prunella vulgaris*. *Antiviral Res.* **1989**, *11*, 263–274.
- (11) Young, S. D.; Britcher, S. F.; Tran, L. O.; Payne, L. S.; Lumma, W. C.; Lyle, T. A.; Huff, J. R.; Anderson, P. S.; Olsen, D. B.; Carroll, S. S.; Pettibone, D. J.; O'Brien, J. A.; Ball, R. G.; Balani, S. K.; Lin, J. H.; Chen, I.-W.; Schleif, W. A.; Sardana, V. V.; Long, W. J.; Byrnes, V. W.; Emini, E. A. L-743,726 (DMP-266): a Novel, Highly Potent Nonnucleoside Inhibitor of the Human Immunodeficiency Virus Type 1 Reverse Transcriptase. *Antimicrob. Agents Chemother.* **1995**, *39*, 2602–2605.
- (12) Hsiou, Y.; Ding, J.; Das, K.; Clark, A. D.; Hughes, S. H.; Arnold, E. Structure of Unliganded HIV-1 Reverse Transcriptase at 2.7 Å Resolution: Implications of Conformational Changes for Polymerization and Inhibition Mechanisms. *Structure* **1996**, *4*, 853–860.
- (13) Eshleman, S. H.; Jackson, J. B. Nevirapine Resistance After Single Dose Prophylaxis. *AIDS Rev.* **2002**, *4*, 59–63.
- (14) Cushman, M.; Golebiewski, M.; Buckheit, R. W., Jr.; Graham, L.; Rice, W. G. Synthesis and Biological Evaluation of an Alkenyldiarylmethane (ADAM) which Acts as a Novel Non-nucleoside HIV-1 Reverse Transcriptase Inhibitor. *Bioorg. Med. Chem. Lett.* **1995**, *5*, 2713–2716.
- (15) Cushman, M.; Casimiro-Garcia, A.; Williamson, K.; Rice, W. G. Synthesis of a Non-Nucleoside Reverse Transcriptase Inhibitor in the Alkenyldiarylmethane (ADAM) Series with Optimized Potency and Therapeutic Index. *Bioorg. Med. Chem. Lett.* **1998**, *8*, 195–198.
- (16) Casimiro-Garcia, A.; Micklatcher, M.; Turpin, J. A.; Stup, T. L.; Watson, K.; Buckheit, R. W., Jr.; Cushman, M. Novel Modifications in the Alkenyldiarylmethane (ADAM) Series of Non-Nucleoside Reverse Transcriptase Inhibitors. *J. Med. Chem.* **1999**, *42*, 4861–4874.
- (17) Xu, G.; Micklatcher, M.; Silvestri, M.; Hartman, T. L.; Burrier, J.; Osterling, M. C.; Wargo, H.; Turpin, J. A.; Buckheit, R. W., Jr.; Cushman, M. The Biological Effects of Structural Variation at the Meta Position of the Aromatic Rings and at the End of the Alkenyl Chain in the Alkenyldiarylmethane Series of Non-Nucleoside Reverse Transcriptase Inhibitors. *J. Med. Chem.* **2001**, *44*, 4092–4113.
- (18) Silvestri, M. A.; Nagarajan, M.; De Clercq, E.; Pannecouque, C.; Cushman, M. Design, Synthesis, Anti-HIV Activities, and Metabolic Stabilities of Alkenyldiarylmethane (ADAM) Non-nucleoside Reverse Transcriptase Inhibitors. *J. Med. Chem.* **2004**, *47*, 3149–3162.
- (19) Deng, B. L.; Cullen, M. D.; Zhou, Z. G.; Hartman, T. L.; Buckheit, R. W.; Pannecouque, C.; De Clercq, E.; Fanwick, P. E.; Cushman, M. Synthesis and Anti-HIV Activity of New Alkenyldiarylmethane (ADAM) Non-nucleoside Reverse Transcriptase Inhibitors (NNRTIs) Incorporating Benzoxazolone and Benzisoxazole Rings. *Bioorg. Med. Chem.* **2006**, *14*, 2366–2374.
- (20) Cullen, M. D.; Deng, B. L.; Hartman, T. L.; Watson, K. M.; Buckheit, R. W.; Pannecouque, C.; De Clercq, E.; Cushman, M. Synthesis and Biological Evaluation of Alkenyldiarylmethane HIV-1 Non-Nucleoside Reverse Transcriptase Inhibitors that Possess Increased Hydrolytic Stability. *J. Med. Chem.* **2007**, *50*, 4854–4867.
- (21) Schäfer, W.; Friebe, W.-G.; Leinert, W.; Mertens, A.; Poll, T.; von der Saal, W.; Zilch, H.; Nuber, H.; Ziegler, M. L. Non-Nucleoside Inhibitors of HIV-1 Reverse Transcriptase: Molecular Modeling and X-ray Structure Investigations. *J. Med. Chem.* **1993**, *36*, 726–732.
- (22) Das, K.; Clark, A. D.; Lewi, P. J.; Heeres, J.; de Jonge, M. R.; Koymans, L. M. H.; Vinkers, H. M.; Daeyaert, F.; Ludovici, D. W.; Kukla, M. J.; De Corte, B.; Kavash, R. W.; Ho, C. Y.; Ye, H.; Lichtenstein, M. A.; Andries, K.; Pauwels, R.; de Bethune, M. P.; Boyer, P. L.; Clark, P.; Hughes, S. H.; Janssen, P. A. J.; Arnold, E. Roles of Conformational and Positional Adaptability in Structure-Based Design of TMC125-R165335 (Etravirine) and Related Non-nucleoside Reverse Transcriptase Inhibitors That Are Highly Potent and Effective Against Wild-Type and Drug-Resistant HIV-1 Variants. *J. Med. Chem.* **2004**, *47*, 2550–2560.
- (23) Das, K.; Lewi, P. L.; Hughes, S. H.; Arnold, E. Crystallography and the Design of Anti-AIDS Drugs: Conformational Flexibility and Positional Adaptability are Important in the Design of Non-Nucleoside HIV-1 Reverse Transcriptase Inhibitors. *Prog. Biophys. Mol. Biol.* **2005**, *88*, 209–231.
- (24) Cushman, M.; Golebiewski, W. M.; Graham, L.; Turpin, J. A.; Rice, W. G.; Fliakas-Boltz, V.; Buckheit, R. W., Jr. Synthesis and Biological Evaluation of Certain Alkenyldiarylmethanes as Anti-HIV-1 Agents Which Act as Non-Nucleoside Reverse Transcriptase Inhibitors. *J. Med. Chem.* **1996**, *39*, 3217–3227.
- (25) Xu, G.; Loftus, T. L.; Wargo, H.; Turpin, J. A.; Buckheit, R. W.; Cushman, M. Solid-Phase Synthesis of the Alkenyldiarylmethane (ADAM) Series of Non-Nucleoside Reverse Transcriptase Inhibitors. *J. Org. Chem.* **2001**, *66*, 5958–5964.
- (26) Silvestri, M. A.; Nagarajan, M.; De Clercq, E.; Pannecouque, C.; Cushman, M. Design, Synthesis, Anti-HIV Activities, and Metabolic Stabilities of Alkenyldiarylmethane (ADAM) Non-nucleoside Reverse Transcriptase Inhibitors. *J. Med. Chem.* **2004**, *47*, 3149–3162.
- (27) Das, K.; Bauman, J. D.; Clark, A. D.; Frenkel, Y. V.; Lewi, P. J.; Shatkin, A. J.; Hughes, S. H.; Arnold, E. High-Resolution Structures of HIV-1 Reverse Transcriptase/TMC278 Complexes: Strategic Flexibility Explains Potency against Resistance Mutations. *Proc. Natl. Acad. Sci. U.S.A.* **2008**, *105*, 1466–1471.
- (28) Himmel, D. M.; Das, K.; Clark, A. D.; Hughes, S. H.; Benjahad, A.; Oumouch, S.; Guillemont, J.; Coupa, S.; Poncelet, A.; Csoka, I.; Meyer, C.; Andries, K.; Nguyen, C. H.; Grierson, D. S.; Arnold, E. Crystal Structures for HIV-1 Reverse Transcriptase in Complexes with Three Pyridinone Derivatives: A New Class of Non-Nucleoside Inhibitors Effective against a Broad Range of Drug-Resistant Strains. *J. Med. Chem.* **2005**, *48*, 7582–7591.
- (29) Jacques, P. S.; Wohrl, B. M.; Ottmann, M.; Darlix, J. L.; Legrice, S. F. J. Mutating the Primer Grip of P66 HIV-1 Reverse-Transcriptase Implicates Tryptophan-229 in Template-Primer Utilization. *J. Biol. Chem.* **1994**, *269*, 26472–26478.
- (30) Ghosh, M.; Jacques, P. S.; Rodgers, D. W.; Ottman, M.; Darlix, J. L.; leGrice, S. F. J. Alterations to the Primer Grip of p66 HIV-1 Reverse Transcriptase and Their Consequences for Template-Primer Utilization. *Biochemistry* **1996**, *35*, 8553–8562.
- (31) Pelemans, H.; Esnouf, R.; De Clercq, E.; Balzarini, J. Mutational Analysis of Trp-229 of Human Immunodeficiency Virus Type 1 Reverse Transcriptase (RT) Identifies this Amino Acid Residue as a Prime Target for the Rational Design of New Non-Nucleoside RT Inhibitors. *Mol. Pharmacol.* **2000**, *57*, 954–960.
- (32) Bauman, J. D.; Das, K.; Ho, W. C.; Baweja, M.; Himmel, D. M.; Clark, A. D.; Oren, D. A.; Boyer, P. L.; Hughes, S. H.; Shatkin, A. J.; Arnold, E. Crystal Engineering of HIV-1 Reverse Transcriptase for Structure-Based Drug Design. *Nucleic Acids Res.* **2008**, *36*, 5083–5092.
- (33) Otwinowski, Z.; Minor, Z. Processing of X-Ray Diffraction Data Collected in Oscillation Mode. *Methods Enzymol.* **1997**, *276*, 307–326.
- (34) Vagin, A.; Teplyakov, A. MOLREP: an Automated Program for Molecular Replacement. *J. Appl. Crystallogr.* **1997**, *30*, 1022–1025.
- (35) Emsley, P.; Cowtan, K. Coot: Model-Building Tools for Molecular Graphics. *Acta Crystallogr., Sect. D: Biol. Crystallogr.* **2004**, *60*, 2126–2132.
- (36) Brunger, A. T.; Adams, P. D.; Clore, G. M.; DeLano, W. L.; Gros, P.; Grosse-Kunstleve, R. W.; Jiang, J. S.; Kuszewski, J.; Nilges, M.; Pannu, N. S.; Read, R. J.; Rice, L. M.; Simonson, T.; Warren, G. L. Crystallography & NMR System: A New Software Suite for Macromolecular Structure Determination. *Acta Crystallogr., Sect. D: Biol. Crystallogr.* **1998**, *54*, 905–921.
- (37) Rice, W. G.; Bader, J. P. Discovery and *In Vitro* Development of AIDS Antiviral Drugs as Biopharmaceuticals. *Adv. Pharmacol. (San Diego)* **1995**, *33*, 389–438.
- (38) Pauwels, R.; Balzarini, J.; Baba, M.; Snoeck, R.; Schols, D.; Herdewijn, P.; Desmyter, J.; De Clercq, E. Rapid and Automated Tetrazolium-based Colorimetric Assay for Detection of Anti-HIV Compounds. *J. Virol. Methods* **1988**, *20*, 309–321.